atoms

MDPI

Article

Constructing Electron-Atom Elastic Scattering Potentials Using Relativistic Coupled-Cluster Theory: A Few Case Studies

Bijaya Kumar Sahoo

Atomic, Molecular and Optical Physics Division, Physical Research Laboratory, Navrangpura, Ahmedabad 380009, India; bijaya@prl.res.in

Abstract: In light of the immense interest in understanding the impact of an electron on atoms in the low-energy scattering phenomena observed in laboratories and astrophysical processes, we propose an approach to construct potentials using relativistic coupled-cluster (RCC) theory for the determination of electron-atom (e-A) elastic scattering cross-sections (eSCs). The net potential of an electron, scattered elastically by an atom, is conveniently expressed as the sum of the static (V_{st}) and exchange (V_{ex}) potentials due to interactions of the scattered electron with the electrons of the atom and potentials due to polarization effects (V_{pol}) on the scattered electron by the atomic electrons. The V_{st} and V_{ex} potentials for the e-A eSC problems can be constructed with a knowledge of the electron density function of the atom, while the V_{pol} potential can be obtained using the polarizabilities of the atom. In this paper, we present the electron densities and electric polarizabilties of Be, Mg, Ne and Ar atoms using two variants of the RCC method. Using these quantities, we construct potentials for e-A eSC problems. To obtain V_{pol} accurately, we evaluate the second- and third-order electric dipole and quadrupole polarizabilities using a linear response approach.

Keywords: coupled-cluster theory; electron scattering; electric polarizabilities

Citation: Sahoo, B.K. Constructing Electron-Atom Elastic Scattering Potentials Using Relativistic Coupled-Cluster Theory: A Few Case Studies. *Atoms* **2022**, *10*, 88. https://doi.org/10.3390/atoms10030088

Academic Editors: Rajesh Srivastava, Dmitry V. Fursa and Grzegorz Piotr Karwasz

Received: 25 July 2022
Accepted: 1 September 2022
Published: 6 September 2022

1. Introduction

The accurate estimation of scattering cross-sections of electrons with atomic systems is of interest for a wide range of applications in laboratory scattering processes and astrophysics [1–4]. The challenge for the calculation of scattering cross-sections lies in determining accurate wave functions for the scattered electron in the vicinity of an atomic target [5,6]. The coupling between the scattered wave functions and atomic wave functions are addressed through the close-coupling [7] and R-matrix [8] formalism, but they are mostly used in a non-relativistic framework [9,10] owing to the complexity involved in the relativistic formalism. In another approach, the interactions among the scattered electron and atomic electrons are included by splitting them into two parts—an electron-electron correlation component and the effects of electron polarization due to the atomic electrons [11–16]. In this approach, the wave functions of the electron and atom are solved separately. The electron correlation effects within the atom are accommodated via a suitable many-body method in the determination of the atomic wave functions (equivalent to atomic wave density functions (ρ)). These functions are further used to construct the interaction potential for the scattered electron. It has both direct and exchange terms owing to the indistinguishable nature of the electrons. An atom is polarized due to the charged scattered electron which modifies the behavior of its wave functions. This effect also influences the construction of the effective potentials of the scattered electrons and is estimated using the electric polarizabilities of the atom. These effective potentials are used to obtain the wave functions of the scattered electrons, for different ranges of kinetic energies, using a distorted wave function (DW) formalism [17,18]. For a highly energetic scattered electron, it is desirable to use the relativistic Dirac equation in the DW approximation (RDW method) [19–22].

In light of several applications of electron-atom scattering cross-sections, such as in modelling metal vapour lasers and plasma plasma environments [23], insights have been gained into different physical processes in many natural and technological environments, including the Earth's atmosphere and in the atmospheres of other planets and their satellites [24], as well as understanding of electron-atom interactions [25]. Theoretical studies on electron scattering by Be, Mg, Ca, Ne, Ar and other atoms have previously been carried out [26–33]. Most of these atoms have closed-shell electronic configurations.

From the above discussion, it is clear that improvement in the accuracy of the scattering cross-section depends on the accurate evaluation of the atomic wave function and the electric polarizabilities of the atom. Typical many-body methods employed to determine the atomic wave functions include a method informed by many-body perturbation theory (MBPT method), the configuration interaction (CI) method, and the coupled-cluster (CC) method. Among these, the CC method is viewed as the "gold standard" for its ability to incorporate electron correlations in the determination of the atomic wave functions at a given approximation level [34–37]. Here, we employ the CC method in a relativistic framework (RCC method) to evaluate the atomic wave functions. Although the (R)CC method has previously been widely applied to calculate many spectroscopic properties to a high degree of accuracy, its ability to obtain scattering cross-sections has not been rigorously tested, except in our first demonstrations in Mg^+ [38] and Ca [39] when studying scattering cross-sections in plasma embedded and confined atom problems. Furthermore, atomic polarization effects on the scattering cross-sections are quite significant. Often, only contributions from the electric dipole polarizabilities (α_d) are considered in the construction of scattering potentials due to their dominant contributions. In recent calculations, it has been shown that contributions arising through the electric quadrupole (α_q) and coupled dipole-quadrupole (B) polarizabilities are non-negligible [15,40]. The aim of the present investigation was to provide general approaches to accurately determine the ρ, α_d, α_q and B values of atomic systems by employing an RCC method that can be used whenever required to obtain the elastic scattering cross-sections of an electron from the closed-shell atomic systems. For representation purposes, we give the results for Be, Ne, Mg and Ar atoms; however, the scheme is very general and can be extended to atomic systems with open-shell configurations.

Apart from the application of electric polarizabilities to determine electron scattering potentials, they are also immensely important for estimating Stark shifts in atomic energy levels. This is why atomic polarizability studies are interesting in their own right. In the literature, α_d has been extensively studied due to its predominant contribution to the energy shift, followed by α_q then B in the presence of an external electric field. Recently, we proposed a linear response approach to determine the α_d, α_q and B values for Zn in the RCC and relativistic normal CC (RNCC) theory frameworks [41]. We had found that the results from the RCC and RNCC theories differed significantly in the commonly considered singles and doubles approximation. Here, we investigate ρ, α_d, α_q and B values using both methods, and compare them with previously reported results for Be, Ne, Mg and Ar atoms. Using these values, we determine the electron scattering potentials and represent these by plotting them against the radial distances. Though these potentials are obtained using a relativistic method, the estimated potentials can be used in both the DW and RDW methods to calculate electron scattering cross-sections with different projectile energies.

2. Theory

For the spherically symmetric interaction potential $V(r)$ of a projectile electron with the target, the direct and exchange scattering amplitudes can be determined by [42]

$$f(k,\theta) = \frac{1}{2\iota k}\sum_{l=0}^{\infty}((l+1)(\exp(2\iota\delta_{\kappa=-l-1})-1) + l(\exp(2\iota\delta_{\kappa=l})-1))P_l(\cos\theta) \quad (1)$$

and

$$g(k,\theta) = \frac{1}{2\imath k}\sum_{l=0}^{\infty}(\exp(2\imath\delta_{\kappa=l}) - \exp(2\imath\delta_{\kappa=-l-1}))P_l^1(\cos\theta) \quad (2)$$

Here k is the relativistic wave number, $\delta_{\kappa=-l-1,l}$ are the scattering phase shifts with $\kappa = -l-1$ and $\kappa = l$ refer to the relativistic quantum numbers for projectile electron with $j = l + 1/2$ and $j = l - 1/2$, respectively. In the above equation, θ is the scattering angle, and $P_l(\cos\theta)$ and $P_l^1(\cos\theta)$ are Legendre polynomials and associated Legendre functions, respectively. Using these amplitudes, the differential cross-sections per unit solid angle for spin unpolarized electrons can be calculated by

$$\frac{d\sigma}{d\Omega} = |f(k,\theta)|^2 + |g(k,\theta)|^2, \quad (3)$$

from which integrated cross-sections can be estimated by integrating over the solid angle. In the (R)DW approximation, the first-order scattering amplitude of an electron from an atomic system with nuclear charge Z and N number of electrons can be expressed as

$$f(J_f,\mu_f;J_i,\mu_i,\theta) = 4\pi^2\sqrt{\frac{k_f}{k_i}}\langle F_{DW}^{k_f}|H_{scat}|F_{DW}^{k_i}\rangle, \quad (4)$$

where J and μ represent the angular momenta of the states of the atomic target and the scattered electron, respectively, k is the momentum of the scattered electron and F_{DF} are the (R)DW wave functions, while the subscript i denotes the initial state and f denotes the final state. A similar expression can be given for g. In the DW method, the effective scattering Hamiltonian in atomic units (a.u.) is given by

$$H_{scat} = -\frac{1}{2}\nabla^2 + V(r) \quad (5)$$

whereas in the RDW method, it is given by

$$H_{scat} = c\alpha\cdot\mathbf{p} + \beta c^2 + V(r). \quad (6)$$

Here c is the speed of light, α and β are the Dirac matrices and $V(r)$ is the scattering potential. For accurate determination of scattering cross-sections, it is imperative to obtain $V(r)$ accurately. In a more convenient form, $V(r)$ can be expressed as [11]

$$V(r) = V_{st}(r) + V_{ex}(r) + V_{pol}(r), \quad (7)$$

where $V_{st}(r)$, $V_{ex}(r)$ and $V_{pol}(r)$ are known as the static, exchange and polarization potentials, respectively. The static potential can have contributions from the nuclear potential ($V_{nuc}(r)$) and the direct electron-electron Coulomb interaction potential $V_C(r)$; i.e., $V_{st}(r) = V_{nuc}(r) + V_C(r)$. Usually, a point-like atomic nucleus is considered in the scattering cross-section calculations by defining $V_{nuc}(r) = -\frac{Z}{r}$ for the atomic number of the system Z. In the present study, we have used the Fermi-charge distribution, given by

$$\rho_A(r) = \frac{\rho_0}{1+e^{(r-c)/a}}, \quad (8)$$

where ρ_0 is the normalization constant, c is the half-charge radius and $a = 2.3/4ln(3)$ is known as the skin thickness, to take into account the finite size effect of the nucleus. This corresponds to the expression for the nuclear potential, as [43]

$$V_{nuc}(r) = -\frac{Z}{\mathcal{N}r} \times \begin{cases} \frac{1}{c}\left(\frac{3}{2} + \frac{a^2\pi^2}{2c^2} - \frac{r^2}{2c^2} + \frac{3a^2}{c^2}P_2^+ \frac{6a^3}{c^2 r}(S_3 - P_3^+)\right) & \text{for } r_i \leq c \\ \frac{1}{r_i}\left(1 + \frac{a62\pi^2}{c^2} - \frac{3a^2 r}{c^3}P_2^- + \frac{6a^3}{c^3}(S_3 - P_3^-)\right) & \text{for } r_i > c, \end{cases} \tag{9}$$

where the factors are

$$\begin{aligned} \mathcal{N} &= 1 + \frac{a^2\pi^2}{c^2} + \frac{6a^3}{c^3}S_3 \\ \text{with} \quad S_k &= \sum_{l=1}^{\infty} \frac{(-1)^{l-1}}{l^k} e^{-lc/a} \\ \text{and} \quad P_k^{\pm} &= \sum_{l=1}^{\infty} \frac{(-1)^{l-1}}{l^k} e^{\pm l(r-c)/a}. \end{aligned} \tag{10}$$

Similarly, we can express $V_C(r) = \sum_{b=1}^{N_e} \langle \phi_b | \frac{1}{|\vec{r} - \vec{r}_b|} | \phi_b \rangle$ with N_e, denoting the total number of electrons of the target atom, and $|\phi_b\rangle$ is the single particle wave function of the atomic electron b such that

$$\frac{1}{|\vec{r}_i - \vec{r}_j|} = \sum_{k=0}^{\infty} \frac{4\pi}{2k+1} \frac{r_<^k}{r_>^{k+1}} \sum_{q=-k}^{k} Y_q^{k*}(\theta, \varphi) Y_q^k(\theta, \varphi), \tag{11}$$

where $r_> = \max(r_i, r_j)$, $r_< = \min(r_i, r_j)$, and $Y_q^k(\theta, \varphi)$ is the spherical harmonics of rank k with its component q. In terms of the Racah operator (C_q^k), the above expression is given by a scalar product as

$$\frac{1}{|\vec{r}_i - \vec{r}_j|} = \sum_{k=0}^{\infty} \frac{r_<^k}{r_>^{k+1}} \mathbf{C}^k(\hat{r}_i) \cdot \mathbf{C}^k(\hat{r}_j). \tag{12}$$

In the Dirac theory, the single particle orbital wave functions are given by

$$|\phi(r)\rangle = \frac{1}{r} \begin{pmatrix} P(r)\chi_{jm_j l_L}(\theta, \varphi) \\ iQ(r)\chi_{jm_j l_S}(\theta, \varphi) \end{pmatrix}, \tag{13}$$

where the upper and lower components are the large and small components of the single particle wave function, respectively, $P(r)$ and $Q(r)$ denote the radial parts of these components, and the χ's denote the spin angular parts of each component which depend on the quantum numbers j, m_j, and l. l_L denotes l for the large component, while l_S denotes l for the small component. Thus, for a closed-shell atomic target, such as those under consideration here, we can have

$$V_C(r) = \sum_b (2j_b + 1) \int_0^{\infty} dr_b \frac{1}{r_>} \Big[P_b^2(r_b) + Q_b^2(r_b) \Big]. \tag{14}$$

It is worth noting that, for open-shell atomic targets, there will be a finite value of multipoles k in the above expression and the computation of $V_C(r)$ will be quite difficult, but is possible [38]. Using density function formalism, the above expression can be given by

$$V_C(r) = \sum_b \left[\frac{1}{r} \int_0^r dr_b \rho_b(r_b) r_b'^2 + \int_r^{\infty} dr_b \rho_b(r_b) r_b \right], \tag{15}$$

where the atomic density function is given by $\hat{\rho}(r) = \sum_i \hat{\rho}_i(r) = \sum_i |\phi_i\rangle\langle\phi_i|$ with

$$\langle \phi_j | \hat{\rho}_i(r) | \phi_k \rangle = \delta_{ji}\delta_{ik} \big(P_j(r) P_k(r) + Q_j(r) Q_k(r) \big). \tag{16}$$

It is not possible to determine $V_{ex}(r)$ separately as it depends on the wave function of the scattered electron itself. However, it can be approximately estimated using the Hara free electron gas model, given by [44]

$$V_{ex}(r) = -\frac{2}{\pi} K_F(r) F[\eta(r)], \tag{17}$$

where the Fermi momentum $K_F(r) = (3\pi\rho(r))^{1/3}$ and $F(\eta) = \frac{1}{2} + \frac{1-\eta^2}{4\eta} ln\left|\frac{1+\eta}{1-\eta}\right|$ with $\eta(r) = \frac{K(r)}{K_F(r)}$ for the local electron momentum given by

$$K^2(r) = K_F^2 + 2I + k^2. \tag{18}$$

Here, I denotes the ionization potential (IP) of the target atom and $k^2/2$ is the kinetic energy of the projectile electron. This means that evaluation of $V_{ex}(r)$ requires the atomic density function and the IP of the atom, along with the kinetic energy of the projectile. Since the kinetic energy of the projectile is arbitrary, we provide here only the $\rho(r)$ values, while IPs can be used from the experimental data.

The polarization potential is given by [45,46]

$$\begin{aligned} V_{pol}(r) &= -\left(\frac{\alpha_d}{2r^4} + \frac{\alpha_q}{2r^6} - \frac{B}{2r^7} + O(1/r^8)\right) \\ &\quad \times \left[1 - e^{(r/r_c)^6}\right], \end{aligned} \tag{19}$$

where α_d, α_q and B are known as the second-order dipole, second-order quadrupole and third-order dipole-quadrupole polarizabilities, respectively. $O(1/r^8)$ corresponds to the higher-order polarizability contributions and is neglected here. r_c is an adjustable parameter, which can be determined by estimating IP using the above potential in the equation of motion, and is assumed to be different for different atoms and also for different levels of approximation in the above expression. For convenience and demonstration purposes, without losing much accuracy, we have considered $r_c = 3.5$ in atomic units (a.u.) for all the atoms considered [46].

In the following section, we present the RCC method to estimate $\rho(r)$, V_{st}, α_d, α_q and B in the closed-shell atomic systems. In place of calculating $V_{st}(r)$ directly using RCC theory, we estimate it by evaluating $V_{nuc}(r)$ and $V_C(r)$ separately with $V_C(r)$ obtained from the $\rho(r)$ values. The expectation values of the operators are again evaluated using the standard RCC and RNCC theory frameworks, and the results are compared with the earlier reported literature values.

3. Methods for Calculations

Since α_d, α_q and B are determined by treating electric dipole operator D and quadrupole operator Q as external perturbations, the atomic wave functions without these external operators are denoted with the superscript 0 ($|\Psi_0^{(0)}\rangle$). We have utilized the Dirac–Coulomb Hamiltonian to determine these unperturbed wave functions, given by

$$H_0 = \sum_{i=1}^{N_e} \left[c\alpha_i \cdot \mathbf{p}_i + (\beta_i - 1)c^2 + V_{nuc}(r_i) + \sum_{j>i} \frac{1}{r_{ij}} \right], \tag{20}$$

where $r_{ij} = |\vec{r}_i - \vec{r}_j|$ is the inter-electronic separation between the electrons located at the r_i and r_j radial positions with respect to the center of the nucleus.

The density matrix of the atomic state $|\Psi_0^{(0)}\rangle$ can be determined by

$$\rho(r) = \frac{\langle\Psi_0^{(0)}|\hat{\rho}(r)|\Psi_0^{(0)}\rangle}{\langle\Psi_0^{(0)}|\Psi_0^{(0)}\rangle}. \tag{21}$$

Following [41], the expressions for α_d, α_q and B of the ground state of a closed-shell system can be given by

$$\begin{aligned} \alpha_d &= 2\frac{\langle\Psi_0^{(0)}|D|\Psi_0^{(d,1)}\rangle}{\langle\Psi_0^{(0)}|\Psi_0^{(0)}\rangle}, \\ \alpha_q &= 2\frac{\langle\Psi_0^{(0)}|Q|\Psi_0^{(q,1)}\rangle}{\langle\Psi_0^{(0)}|\Psi_0^{(0)}\rangle} \end{aligned} \tag{22}$$

and

$$B = 2\frac{\langle\Psi_0^{(d,1)}|D|\Psi_0^{(q,1)}\rangle}{\langle\Psi_0^{(0)}|\Psi_0^{(0)}\rangle}, \tag{23}$$

where $|\Psi_0^{(0)}\rangle$ and $|\Psi_0^{(o,1)}\rangle$ are the zeroth-order wave function and the first-order wave function of the atom due to an operator $O \equiv D$ or Q.

From the above expressions, it is clear that accurate evaluations of α_d, α_q and B depend on the many-body method employed to determine $|\Psi_0^{(0)}\rangle$ and $|\Psi_0^{(o,1)}\rangle$. These wave functions can be determined by solving the following equations

$$H_0|\Psi_0^{(0)}\rangle = E_0^{(0)}|\Psi_0^{(0)}\rangle \tag{24}$$

and

$$(H_0 - E_0^{(0)})|\Psi_0^{(o,1)}\rangle = (E_0^{(o,1)} - O)|\Psi_0^{(0)}\rangle \tag{25}$$

with the first-order energy correction $E_0^{(o,1)}$ due to O, which is zero in the present study.

Our intention here is to demonstrate the evaluation of $\rho(r)$, α_d, α_q and B in the closed-shell atoms using the RCC and RNCC theories to construct the electron-atom scattering potentials. In the RCC theory, we can express [47,48]

$$|\Psi_0^{(0)}\rangle = e^{T^{(0)}}|\Phi_0\rangle, \tag{26}$$

and

$$|\Psi_0^{(o,1)}\rangle = e^{T^{(0)}}T^{(o,1)}|\Phi_0\rangle, \tag{27}$$

where $T^{(0)}$ accounts for electron correlation effects, and $T^{(o,1)}$ includes electron correlations, along with the effect due to O, while acting on the Dirac–Hartree–Fock (DHF) wave function $|\Phi_0\rangle$ of the system.

In this approach, the expressions for ρ, α_d, α_q and B are given by [41]

$$\rho(r) = \frac{\langle\Phi_0|e^{T^{(0)\dagger}}\hat{\rho}(r)e^{T^{(0)}}|\Phi_0\rangle}{\langle\Phi_0|e^{T^{(0)\dagger}}e^{T^{(0)}}|\Phi_0\rangle}, \tag{28}$$

$$\alpha_d = 2\frac{\langle\Phi_0|e^{T^{(0)\dagger}}De^{T^{(0)}}T^{(d,1)}|\Phi_0\rangle}{\langle\Phi_0|e^{T^{(0)\dagger}}e^{T^{(0)}}|\Phi_0\rangle}, \tag{29}$$

$$\alpha_q = 2\frac{\langle\Phi_0|e^{T^{(0)\dagger}}Qe^{T^{(0)}}T^{(q,1)}|\Phi_0\rangle}{\langle\Phi_0|e^{T^{(0)\dagger}}e^{T^{(0)}}|\Phi_0\rangle} \tag{30}$$

and

$$B = 2\frac{\langle\Phi_0|T^{(d,1)\dagger}e^{T^{(0)\dagger}}De^{T^{(0)}}T^{(q,1)}|\Phi_0\rangle}{\langle\Phi_0|e^{T^{(0)\dagger}}e^{T^{(0)}}|\Phi_0\rangle}. \tag{31}$$

Evaluating the above expressions involves two major challenges, even after making approximations in the level of excitations in the RCC calculations. The first being that there are two non-terminating series in the numerator and denominator. The second challenge is that the numerator can have factors which are both connected and disconnected to the operators D or Q. These problems can be partially addressed by defining a normal-order form of operators with respect to $|\Phi_0\rangle$, in which the above expressions can be simplified to [49,50]

$$\rho(r) = \langle\Phi_0|e^{T^{(0)\dagger}}\hat{\rho}(r)e^{T^{(0)}}T^{(d,1)}|\Phi_0\rangle_c, \quad (32)$$

$$\alpha_d = 2\langle\Phi_0|e^{T^{(0)\dagger}}De^{T^{(0)}}T^{(d,1)}|\Phi_0\rangle_c, \quad (33)$$

$$\alpha_q = 2\langle\Phi_0|e^{T^{(0)\dagger}}Qe^{T^{(0)}}T^{(q,1)}|\Phi_0\rangle_c \quad (34)$$

and

$$B = 2\langle\Phi_0|T^{(d,1)\dagger}e^{T^{(0)\dagger}}De^{T^{(0)}}T^{(q,1)}|\Phi_0\rangle_c, \quad (35)$$

where subscript c denotes connected terms only appearing within the respective expression. Although this removes the non-terminating series appearing in the denominator, it still contains a non-terminating series in the numerator. Further, the above expressions with connected terms hold good only when there is no approximation made in the T operator. In practice, T is truncated as for our RCCSD method. These expressions again do not satisfy the Hellman–Feynman theorem [34]. All these problems can be circumvented by the RNCC theory.

In the RNCC theory, the ket state is the same as in RCC theory but the bra state is replaced by

$$\langle\tilde{\Psi}^{(0)}| = \langle\Phi_0|(1+\Lambda^{(0)})e^{-T^{(0)}}, \quad (36)$$

with a de-excitation operator $\Lambda^{(0)}$ that satisfies

$$\langle\tilde{\Psi}^{(0)}|\Psi^{(0)}\rangle = \langle\Phi_0|(1+\Lambda^{(0)})e^{-T^{(0)}}e^{T^{(0)}}|\Phi_0\rangle = 1. \quad (37)$$

It can be shown that the eigenvalues of both $\langle\Psi^{(0)}|$ and $\langle\tilde{\Psi}^{(0)}|$ are the same if

$$\langle\Phi_0|\Lambda\bar{H}_0|\Phi_0\rangle = 0, \quad (38)$$

where $\bar{H} = e^{-T^{(0)}}H_0e^{T^{(0)}} = (He^T)_c$.

Now, we can write the first-order perturbed wave function in the RNCC theory as [41,51]

$$\langle\tilde{\Psi}^{(o,1)}| = \langle\Phi_0|\left[\Lambda^{(o,1)} + (1+\Lambda^{(0)})T^{(o,1)}\right]e^{-T^{(0)}}. \quad (39)$$

Consequently, the RNCC expressions for $\rho(r)$, α_d, α_q and B are given by

$$\rho(r) = \langle\Phi_0|\left(1+\Lambda^{(0)}\right)\tilde{\rho}(r)|\Phi_0\rangle, \quad (40)$$

$$\alpha_d = \langle\Phi_0|\left(1+\Lambda^{(0)}\right)\tilde{D}T^{(d,1)} + \Lambda^{(d,1)}\tilde{D}|\Phi_0\rangle, \quad (41)$$

$$\alpha_q = \langle\Phi_0|\left(1+\Lambda^{(0)}\right)\tilde{Q}T^{(q,1)} + \Lambda^{(q,1)}\tilde{Q}|\Phi_0\rangle \quad (42)$$

and

$$B = \langle\Phi_0|\Lambda^{(d,1)}\tilde{D}T^{(q,1)} + \Lambda^{(q,1)}\tilde{D}T^{(d,1)}|\Phi_0\rangle, \quad (43)$$

where $\tilde{O} = (Oe^{T^{(0)}})_c$. In the RNCC theory, we also consider only the singles and doubles excitations (RNCCSD method) to carry out the calculations. It is worth noting

here that the next leading-order electron correlation effects to $\rho(r)$, α_d, α_q and B arising through the higher-level excitations will converge faster in the RNCC theory than the RCC theory [41,51].

4. Results and Discussion

We first evaluate the density functions $\rho(r)$ of the ground states of the Be, Mg, Ne and Ar atoms. Since the correlation contributions, i.e.,the differences between the DHF and RCC/RNCC values (given as $\delta\rho(r)$), to these functions are very small compared to the DHF values, we consider these contributions separately. In Figure 1, we plot $\rho(r)$ values from the DHF method, while the correlation contributions $\delta\rho(r)$ from the RCCSD and RNCCSD methods are shown in Figure 2. As can be seen from the first figure, the density profiles of Be, Mg, Ne and Ar appear to be different. This suggests that the electronic charge distributions among these atoms are quite different. From the second figure, we see that there are slight differences in the correlation contributions from the RCCSD and RNCCSD methods in Be, while, for the other atoms, not much difference is observed. As mentioned earlier, accurate values of α_d, α_q and B are important in determining $V_{pol}(r)$ for the electron-atom scattering problem. Therefore, the roles of the electron correlation effects through the RCCSD and RNCCSD methods in the above atoms can be better understood through the calculation of electric polarizabilities.

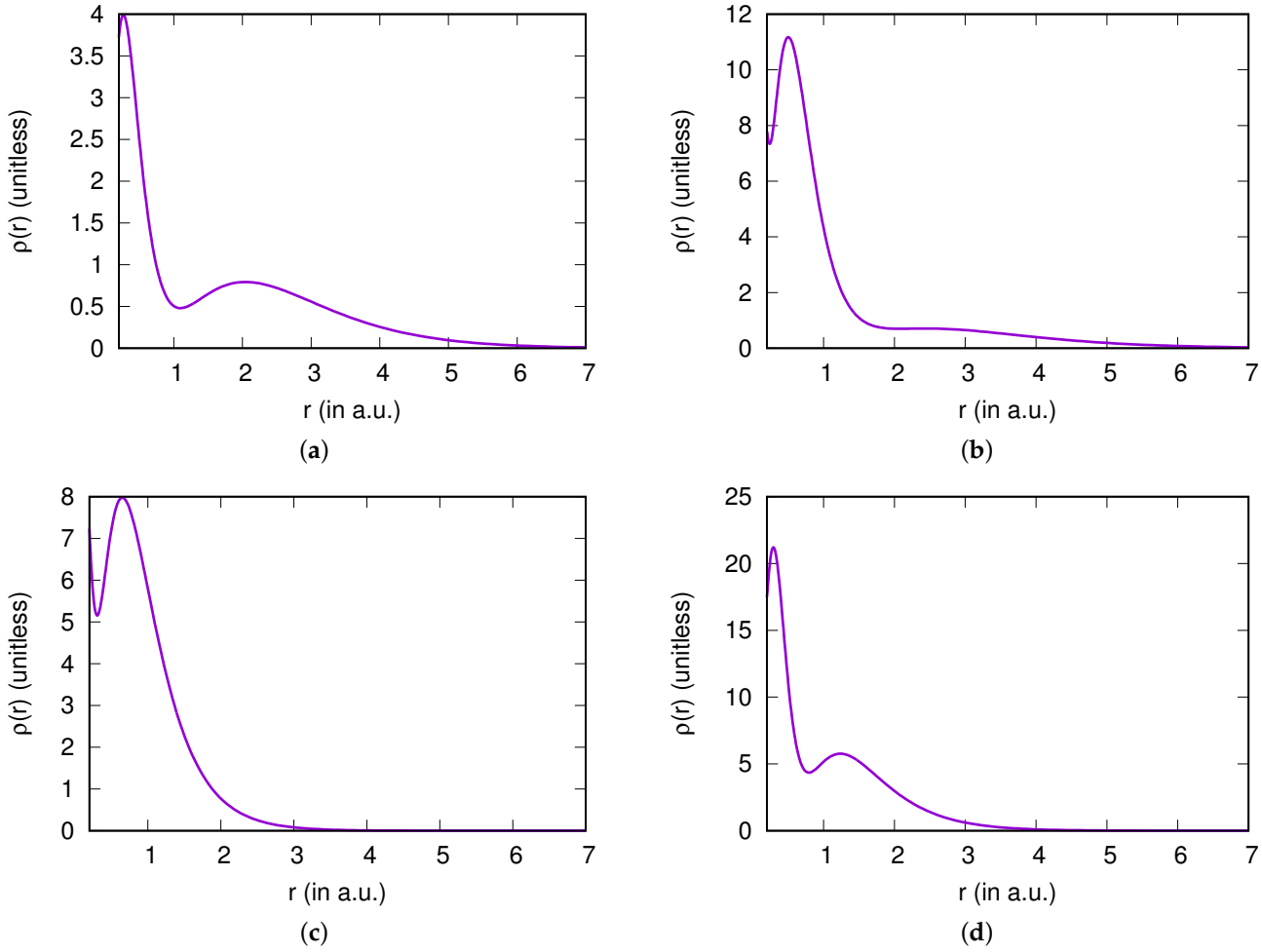

Figure 1. Densityprofiles of (**a**) Be, (**b**) Mg, (**c**) Ne and (**d**) Ar atoms obtained using the DHF method in their ground states. The radial distances (r) are given in atomic units (a.u.), while density values ρ(r) are unitless.

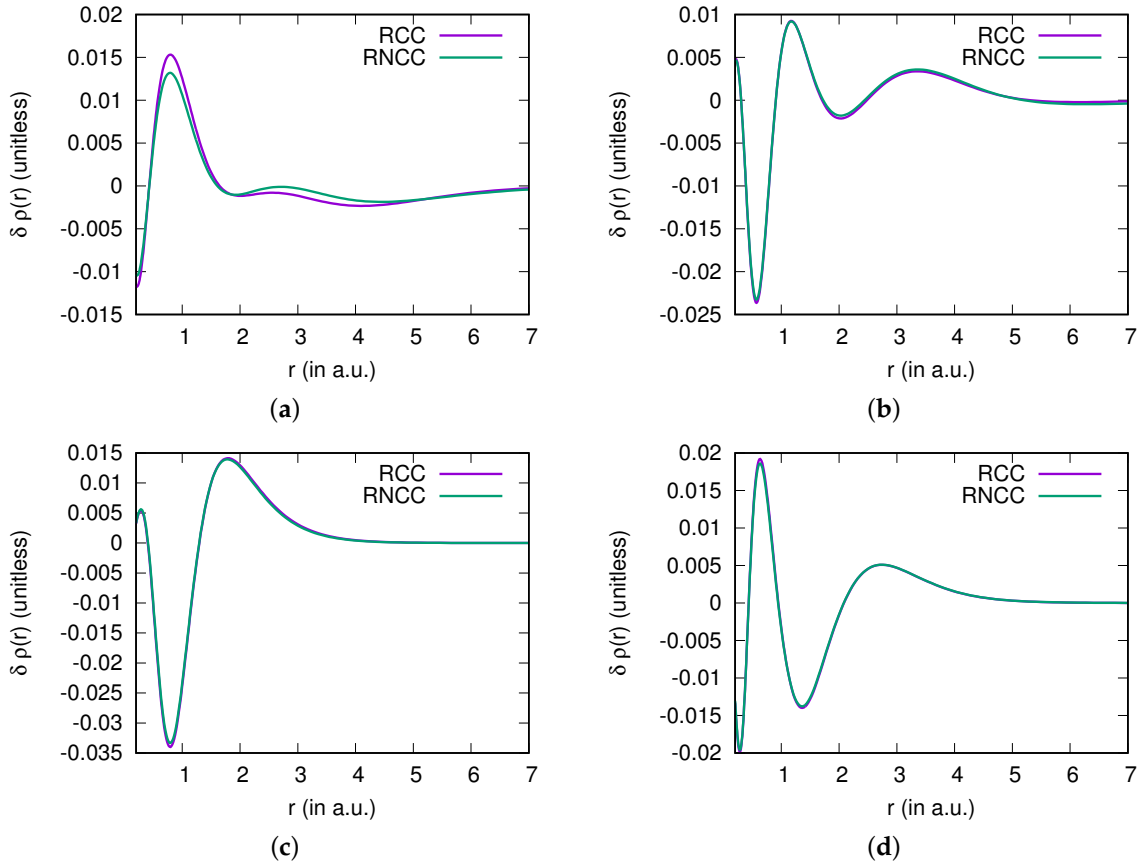

Figure 2. Correlation contributions to $\rho(r)$ (shown in figure as $\delta\rho(r)$) from the RCC and RNCC methods in (**a**) Be, (**b**) Mg, (**c**) Ne and (**d**) Ar. As seen, the $\delta\rho(r)$ values are almost the same through the RCC and RNCC methods in all atoms except Be in which slight differences are evident.

To our knowledge, there are no available calculations of $\rho(r)$ of the atoms considered which explicitly use the (R)CC methods previously discussed. In a recent study [52], a CI method was employed in a non-relativistic framework to determine density functions for studying the quantum potential neural network of Li, Be and Ne atoms. We found that the density function behaviors we obtained for Be and Ne almost matched those of the density functions of these atoms reported in [52]. We could not find any reference which specifically reported the density functions of Mg and Ar; however, from analyses of radial function distributions in Ne and Ar shown in [53], we assume that the behavior of the density functions of the Ar atom we obtained using the DHF method follow the correct trend. Moreover, in a different investigation [54], calculations of the $\rho(r)$ values in carbon atoms followed similar trends to our results for Mg. From all these analyses, we infer that our $\rho(r)$ values for Mg should be correct. Since the previous studies did not explicitly discuss $\delta\rho(r)$ contributions, we were unable to compare our findings for these values with any other calculations.

In Table 1, we present the α_d, α_q and B values calculated using the DHF, RCCSD and RNCCSD methods. It can be seen from this table that there are large differences between the results from the DHF and RCCSD methods. These differences become larger in the determination of α_q followed by the B values. The RCCSD values of B in the alkaline-earth atoms are about 2.5 times larger than the DHF values. In all atoms, the RNCCSD values of α_d, α_q and B are seen to be lower than the RCCSD values, except in the determination of α_q in the Be atom. The α_d values from the RCCSD and RNCCSD methods are very close to each other, but there are significant differences observed among the α_q values of the RCCSD and RNCCSD methods. These differences are quite prominent in the evaluation of the B values. As discussed in the previous section, an approximated RNCC method is

more reliable in the determination of properties than an approximated RCC method; thus, we believe that our RNCCSD results are more accurate and should be treated here as the final results.

Table 1. Our calculated values of α_d, α_q and B (in a.u.) of the Be, Mg, Ne and Ar atoms from the DHF, RCCSD and RNCSSD methods. These values are also compared with precise values from the literature.

Property	DHF	RCCSD	RNCCSD	Others
		Be atom		
α_d	30.53	38.33	37.40	37.739(30) [55] 37.76(22) [56] 37.86(17) [57] 37.74(3) [58]
α_q	220.15	299.82	304.34	300.96 [55] 300.6(3) [56]
B	−1218.38	−2729.17	−2172.95	−2100(60) [55]
		Mg atom		
α_d	54.94	71.74	69.40	71.22(36) [55] 71.3(7) [56] 72.54(50) [57] 71.2(4) [58]
α_q	567.37	809.56	797.91	813.9(16.3) [55] 812(6) [56]
B	−3847.89	−9293.74	−7226.24	−7750(780) [55]
		Ne atom		
α_d	1.98	2.70	2.62	2.6669(8) [59] 2.652(15) [57] 2.66110(3) [58] 2.64 [60]
α_q	4.76	7.48	7.09	7.52(15) [55] 7.36 [60]
B	−6.15	−14.38	−11.67	−18.12(54) [55] −17.27 [60]
		Ar atom		
α_d	10.15	11.21	11.15	11.083(7) [61] 11.070(7) [62] 11.089(4) [57] 11.083(7) [58] 11.33 [63] 10.73 [64]
α_q	37.19	51.61	50.33	53.37(1.07) [55] 53.22 [63] 49.46 [64]
B	−71.07	−140.53	−115.35	−159(8) [55] −167.5 [63] −141 [64]

Due to the enormously wide use of electric polarizabilities in various experimental applications, a number of theoretical calculations have been presented in the literature. We consider the results obtained from previous experiments [59,61,62], sources that provide compilations of earlier data [55,58], our own previous RCC calculations [57], and evidence cited in papers that report most of these quantities using a single many-body method [56,60,63,64]. The results of other studies are mostly summarized in [55,58]. Many earlier theoretical studies determined the α_d values, with less theoretically based results found for the α_q values of the atoms considered. To our knowledge, only a few non-relativistic calculations for the B values of the Be, Mg, Ne and Ar atoms considered have been reported [55,60,63,64]. Furthermore, we did not find any experimental results of α_d for Be and Mg, but precisely measured α_d values are available for Ne and Ar. Both of our RCCSD and RNCSSD values are in agreement with those obtained from previous calculations. We note that our RCCSD value of α_q is closer to the previously reported precise calculation result than the RNCCSD value; however, this trend is different for the

α_d and B values. These findings are slightly different for the Mg atom, where it is observed that both the α_d and α_q values from our RCCSD method closely matched the previously reported accurate calculations, but the RNCCSD value for B was in closer agreement with the previous calculation [55]. From these comparisons, it is not possible to argue that the RCCSD method values are more accurate than the RNCCSD results wherever they agree with the previous calculations unless they are verified experimentally. The α_q and B values, previously estimated using a finite-field (FF) approach, are not numerically reliably. The experimental value of α_d in Ne is very precise, and comparison of theoretical results with this value can indicate the validity of the many-body methods employed. We also compared our RNCCSD values of α_d and α_q with the literature values in Table 1. For Be, there are several calculations of α_d available; we have listed some of the precise theoretical results in the above table from the CC and RCC calculations. Several calculations of α_q of the considered atoms, including Be, have been reported using non-relativistic variation-perturbation methods using a finite-field (FF) approach [55,60,63,64], and using a combined CI and MBPT (CI + MBPT) method in a sum-over-states approach [56]. Our RNCCSD α_d value closely matches the previously estimated values. We found a slight difference for the α_q value from the RNCCSD method and the previously reported precise value using the CI + MBPT method [56]. Our RCCSD value of α_d in Mg agrees closely with the previously calculated values using various many-body methods. However, the previously reported α_d values from different calculations spread over a wide-range. This is due to the large electron correlation effects exhibited by both the valence electrons of the Mg atom. Nonetheless, our RNCCSD value of α_d is also close to that obtained from other calculations. However, our RCCSD value for α_q is closer to previous calculations while the RNCCSD result differs significantly from the earlier calculations. From this difference, we cannot say with confidence that the RCCSD value is more accurate than the RNCCSD result. This is because the earlier predicted α_q values are obtained using non-relativistic methods or lower-order relativistic methods. Thus, only empirical measurements can confirm the reliability of these calculations. Comparing the α_d value of Ne with experiment [59], our RCCSD value is closer to the experimental value than the RNCCSD value. We anticipate that after including Breit and quantum electrodynamic corrections, the RNCCSD value will improve further. Similarly, the α_q value from the RCCSD method is closer to the previous calculations than the RNCCSD method. Since there is no experimental result for α_q available, we cannot claim that the RNCCSD value is less accurate than the RCCSD result. Similar trends for the α_d and α_q values can be seen in the Ar atom.

Compared to the α_d and α_q values, B values have received little attention both in theoretical and experimental studies. The contributions of these values to the Stark effects are extremely small when being precisely observed. Strong electron correlation effects are also involved when evaluating B values accurately. In addition, extrapolation of B values from the FF approach requires inclusion of both the electric dipole and quadrupole field interactions in the atomic Hamiltonian. In the linear response approach, estimations of the B values demand calculation of first-order perturbed wave functions due to both the electric dipole and quadrupole operators. These are the main reasons why the B values are not widely investigated in many atomic systems. We identified some literature values for B of the Be, Mg, Ne and Ar atoms [55,60,63,64] which are listed in Table 1. These literature values are obtained by adopting an FF approach in a non-relativistic framework. By comparison of our calculations with literature values, we note that our RNCCSD values agree with the earlier reported values, while the RCCSD results differ greatly for both the Be and Mg atoms. However, this is reversed for the Ne and Ar atoms. The reason for this could be that different many-body methods were considered to estimate the B values of the alkaline-earth atoms and of the noble gas atoms. We assume that our RNCSSD results are more reliable compared to all the listed values in Table 1.

In Figure 3a,b, we show the individual contributions to $V(r)$ from the RCCSD and RNCCSD methods for the Be atom. As can be seen in both these plots, the contributions from V_{nuc} dominates while the V_C contributions are also quite visible. There are also

noticeable contributions arising from the $V_{pol}(r)$. Similar trends can also be observed for the RCCSD values, as shown in Figure 3c, and the RNCCSD values, as shown in Figure 3d, for the Mg atom, but the shapes are slightly different due to $V_C(r)$ and $V_{pol}(r)$ contributions. These differences can be understood from the density profiles of both the atoms shown in Figure 1. In Figure 4a–d, we show different contributions to $V(r)$ from the RCCSD and RNCCSD methods for Ne and Ar. As can be seen from the figure, the trends from individual contributions to $V(r)$ in both Ne and Ar appear quite similar except for their magnitudes. The figure also shows that contributions from $V_{pol}(r)$ are negligibly small in both the atoms. Compared to the alkaline-earth atoms, the results for both the Ne and Ar atoms look quite similar to those for the Mg atom. It is of note that the density profiles shown in Figure 1 of the Be and Ar atoms appear similar, while the density profiles of Mg and Ne appear to have similar features. Thus, it is not possible to obtain a clear picture of the scattering potential behavior of an electron from an atom just by looking at the density profile of the atom. Nonetheless, we have discussed procedures to construct the electron-atom scattering potentials by evaluating contributions from the static and polarization potentials due to the Be, Mg, Ne and Ar atoms using the RCC and RNCC methods. These procedures can also be adopted for heavier closed-shell atomic systems, where electron correlation effects could be very pronounced.

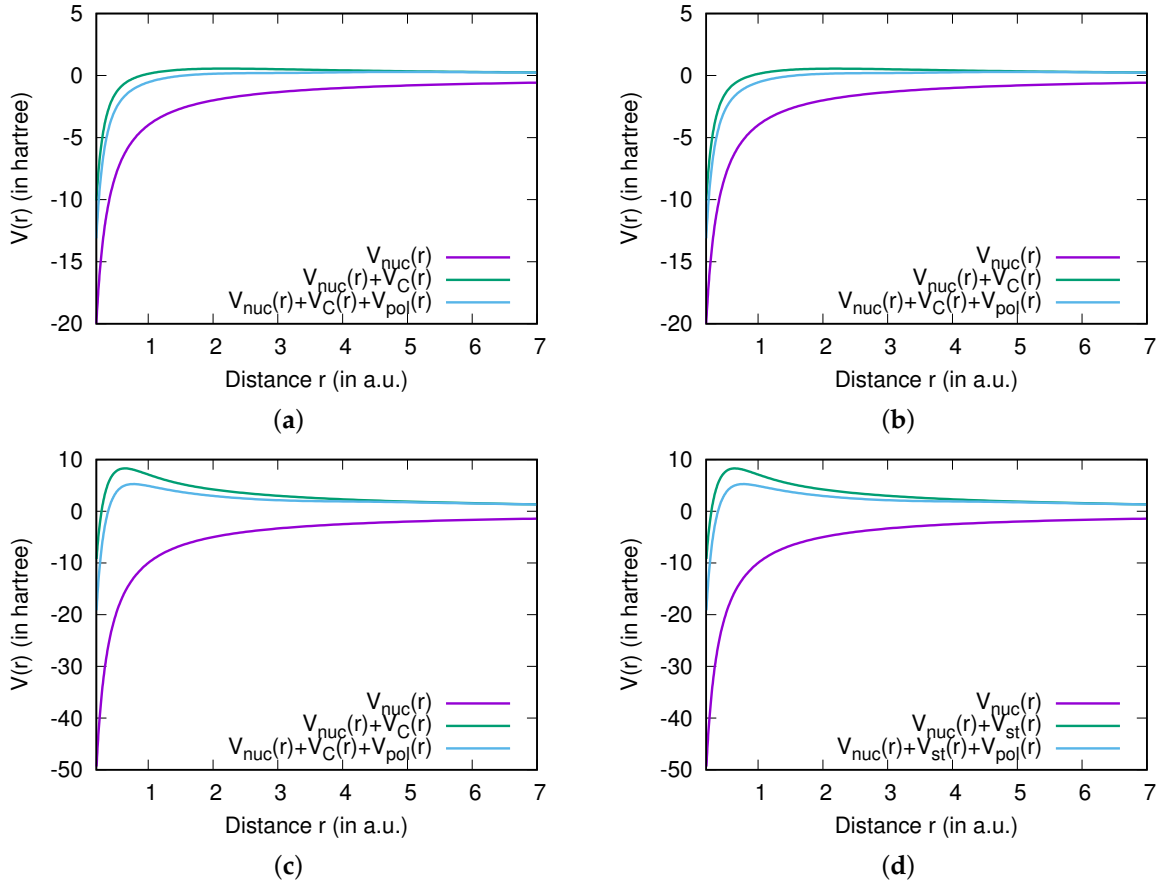

Figure 3. Plots demonstrating comparative analyses of contributions from $V_{nuc}(r)$, $V_C(r)$ and $V_{pol}(r)$ to the electron scattering potential $V(r)$ from the Be and Mg alkaline-earth atoms. In (**a**,**b**), results are given from the RCCSD and RNCCSD methods, respectively, for the Be atom. Results from the RCCSD and RNCCSD methods are shown in (**c**,**d**), respectively, for the Mg atom. All quantities are given in a.u.

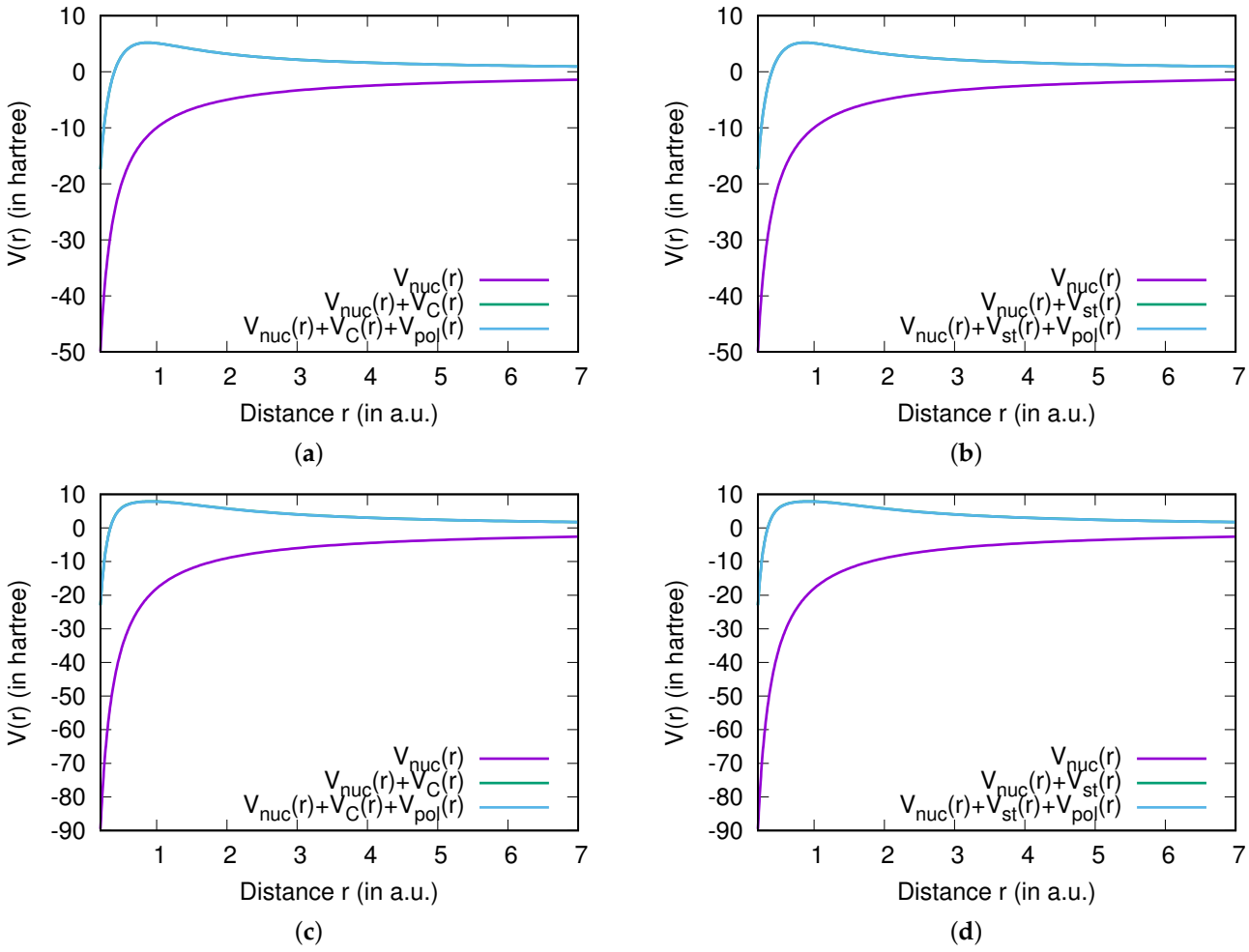

Figure 4. Plots demonstrating different contributions to $V(r)$ from the Ne and Ar noble atoms. In (**a**,**b**), results are given from the RCCSD and RNCCSD methods, respectively, for the Ne atom, while the results from the RCCSD and RNCCSD methods for the Ar atom are shown in (**c**,**d**), respectively. All quantities are given in a.u.

5. Conclusions

We have demonstrated approaches employing relativistic-coupled cluster theory to determine potentials for the evaluation of electron-atom elastic scattering cross-sections. For this purpose, we considered both the standard and normal versions of the relativistic coupled-cluster theory in the singles and doubles approximation, and presented results for the Be, Mg, Ne and Ar atoms as representative elements for the alkaline-earth and noble gas atoms of the Periodic Table. To estimate the static potential contributions, the finite-size nuclear effect was determined through the nuclear potential, while the two-electron correlation effects were estimated using relativistic coupled-cluster theory. The density functions of the above atoms from both the considered relativistic coupled-cluster theories were presented to estimate the Coulomb exchange potential contributions, which we neglected here for estimating potentials. Furthermore, we determined the electric dipole, quadrupole and dipole-quadrupole polarizabilities to account for the electron polarization effects on the scattering potential. The results from both the standard and normal relativistic coupled-cluster theories were compared with the literature values. These methods can be further applied to other heavier atomic systems to study electron-atom scattering cross-sections more accurately where the electron correlation effects within the atom will be more prominent than for the lighter elements investigated here.

Funding: This research received no external funding.

Acknowledgments: We acknowledge use of the Vikram-100 HPC cluster of the Physical Research Laboratory (PRL), Ahmedabad, India for the computations.

Conflicts of Interest: The author declares no conflict of interest.

References

1. Johnson, R.E. *Introduction to Atomic and Molecular Collisions*; Plenum Press: New York, NY, USA; London, UK, 1982.
2. Amusia, M.Y. Many-body atomic physics, Chapter 8. In *Many-Body Effects in Single Photoionization Processes*; Boyle, J.J., Pindzola, M.S., Eds.; Cambridge University Press: New York, NY, USA, 1998; p. 185.
3. Kotlarchyk, M. *Encyclopedia of Spectroscopy and Spectrometry*; Lindon, J.C., Ed.; Elsevier: Oxford, UK, 1999; pp. 2074–2084.
4. Pradhan, A.K.; Nahar, S.N. *Atomic Astrophysics and Spectroscopy*; Cambridge University Press: New York, NY, USA, 2011.
5. Dressler, R.A.; Chiu, Y.-H.; Zatsarinny, O.; Bartschat, K.; Srivastava, R.; Sharma, L. Near-infrared collisional radiative model for Xe plasma electrostatic thrusters: The role of metastable atoms. *J. Phys. D* **2009**, *42*, 185203. [CrossRef]
6. Dipti; Gangwar, R.K.; Srivastava, R.; Stauffer, A.D. Collisional-radiative model for non-Maxwellian inductively coupled argon plasmas using detailed fine-structure relativistic distorted-wave cross sections. *Eur. Phys. J. D* **2013**, *67*, 40244.
7. Bray, I.; Fursa, D.V.; Kheifets, A.S.; Stelbovics, A.T. Electrons and photons colliding with atoms: Development and application of the convergent close-coupling method. *J. Phys. B* **2002**, *35*, R117. [CrossRef]
8. Burke, P.G. *R-Matrix Theory of Atomic Collisions*; Springer: Berlin/Heidelberg, Germany, 2013.
9. Post, D.E. A review of recent developments in atomic processes for divertors and edge plasmas. *J. Nucl. Mater.* **1995**, *220*, 143–157. [CrossRef]
10. Jablonski, A.; Salvat, F.; Powell, C.J. Comparison of Electron Elastic-Scattering Cross Sections Calculated from Two Commonly Used Atomic Potentials. *J. Phys. Chem. Ref. Data* **2004**, *33*, 409–451. [CrossRef]
11. O'Connell, J.K.; Lane, N.F. Nonadjustable exchange-correlation model for electron scattering from closed-shell atoms and molecules. *Phys. Rev. A* **1983**, *27*, 1893. [CrossRef]
12. Yuan, J.; Zhang, Z. The low-lying shape resonances in low-energy electron scattering with Be, Mg and Ca atoms. *J. Phys. B At. Mol. Opt. Phys.* **1989**, *22*, 2751. [CrossRef]
13. Franz, J. Positron-electron correlation-polarization potentials for the calculation of positron collisions with atoms and molecules. *Eur. Phys. J. D* **2017**, *71*, 44. [CrossRef]
14. Tenfen, W.; Barp, M.V.; Arretche, F. Low-energy elastic scattering of positrons by O_2. *Phys. Rev. A* **2019**, *99*, 022703. [CrossRef]
15. Arretche, F.; Andermann, A.M.; Seidel, E.P.; Tenfen, W.; Sahoo, B.K. Polarization effects, shape resonances and bound states in low energy positron elastic scattering by Zinc and Cadmium vapours. *J. Electron Spectrosc. Relat. Phenom* **2022**, *254*, 147186. [CrossRef]
16. Khandker, M.H.; Haque, A.K.F.; Haque, M.M.; Billah, M.M.; Watabe, H.; Uddin, M.A. Relativistic Study on the Scattering of $e^{\pm}$ from Atoms and Ions of the Rn Isonuclear Series. *Atoms* **2021**, *9*, 59. [CrossRef]
17. Miller, W.H. Distorted-Wave Theory for Collisions of an Atom and a Diatomic Molecule. *J. Chem. Phys.* **1968**, *49*, 2373–2381. [CrossRef]
18. Madison, D.H.; Shelton, W.N. Distorted-Wave Approximation and Its Application to the Differential and Integrated Cross Sections for Electron-Impact Excitation of the $2\,^1P$ State of Helium. *Phys. Rev. A* **1973**, *7*, 499. [CrossRef]
19. Toshima, N.; Eichler, J. Distorted-wave approximations for relativistic atomic collisions. *Phys. Rev. A* **1990**, *41*, 5221. [CrossRef]
20. Srivastava, R.; Muktavat, K.; Stauffer, A.D. Electron Impact Excitation of Atoms in the Relativistic Distorted Wave Approximation. *Phys. Scr.* **2004**, *2004*, 241. [CrossRef]
21. Sharma, L.; Surzhykov, A.; Srivastava, R.; Fritzsche, S. Electron-impact excitation of singly charged metal ions. *Phys. Rev. A* **2011**, *83*, 062701. [CrossRef]
22. Marucha, A.M.; Kariuki, P.K.; Okumu, J.; Singh, C.S. Relativistic distorted wave approach to electron impact excitation of argon gas using a complex potential. *J. Phys. Commun.* **2021**, *5*, 075011. [CrossRef]
23. Teubner, P.J.O.; Farrell, P.M.; Karaganov, V.; Law, M.R.; Suvorov, V. Laser Assisted Collisions of Electrons with Metal Vapours. *Aust. J. Phys.* **1996**, *49*, 481–498. [CrossRef]
24. Joshipura, K.; Mason, N. *Atomic-Molecular Ionization by Electron Scattering: Theory and Applications*; Cambridge University Press: New York, NY, USA, 2019; pp. 177–218.
25. Buckman, S.J.; Cooper, J.W.; Elford, M.T.; Inokuti, M.; Itikawa, Y.; Tawara, H. *Interactions of Photons and Electrons with Atoms*; Itikawa, Y., Ed.; Springer: Berlin/Heidelberg, Germany, 2000; Volume 17A, pp. 1–77.
26. Jhanwar, B.L.; Khare, S.P.; Kumar, A., Jr. Elastic scattering of electrons on Ne atoms at intermediate energies. *J. Phys. B At. Mol. Phys.* **1978**, *11*, 887. [CrossRef]
27. Khare, S.P.; Kumar, A., Jr. Elastic scattering of electrons by argon atoms. *Pramana* **1978**, *10*, 63–73. [CrossRef]
28. Khare, S.P.; Kumar, A.; Lata, K. Elastic scattering of electrons and positrons by magnesium atoms at intermediate energies. *J. Phys. B At. Mol. Phys.* **1983**, *16*, 4419. [CrossRef]
29. Elkilany, S.A. Elastic scattering of electrons by helium and neon atoms. *Nouv. Cim. D* **1998**, *20*, 147–154. [CrossRef]
30. Phelps, A.V.; Greene, C.H.; Burke, J.P., Jr.; Phelps, A.V. Collision cross sections for argon atoms with argon atoms for energies from 0.01 eV to 10 keV. *J. Phys. B At. Mol. Opt. Phys.* **2000**, *33*, 2965. [CrossRef]

31. Khoperskiĭ, A.N.; Yavna, V.A.; Nadolinskiĭ, A.M.; Dzyuba, D.V. Elastic scattering of a photon by the neon atom near the K ionization edge. *Opt. Spectrosc.* **2004**, *96*, 195–197. [CrossRef]
32. Baynard, T.; Reber, A.C.; Niedziela, R.F.; Darveau, S.A.; Prutzman, B.; Berry, R.S. Electron-Atom Superelastic Scattering in Magnesium at Millielectron Volt Energies. *J. Phys. Chem. A* **2007**, *111*, 12487–12494. [CrossRef] [PubMed]
33. Kumar, A.; Kumar, S.; Rastogi, N.; Raj, D. Critical points for electron-Mg atom elastic scattering. *J. Phys. B At. Mol. Opt. Phys.* **2018**, *51*, 035203. [CrossRef]
34. Bishop, R.; Arponen, J.; Pajanee, P. *Aspects of Many-Body Effects in Molecules and Extended Systems*; Springer: Berlin/Heidelberg, Germany, 1989.
35. Szabo, A.; Ostuland, N. *Modern Quantum Chemistry*, 1st ed. (revised); Dover Publications, Inc.: Mineola, NY, USA, 1996.
36. Crawford, T.D.; Schaefer, H.F., III. *An Introduction to Coupled Cluster Theory for Computational Chemists*; Lipkowitz, K.B., Boyd, D.B., Eds.; Wiley: New York, NY, USA, 2000; pp. 33–136.
37. Shavitt, I.; Bartlett, R.J. *Many-Body Methods in Chemistry and Physics*; Cambidge University Press: Cambridge, UK, 2009.
38. Sharma, L.; Sahoo, B.K.; Malkar, P.; Srivastava, R. Application of relativistic coupled-cluster theory to electron impact excitations of Mg^+ in the plasma environment. *Eur. Phys. J. D* **2018**, *72*, 10. [CrossRef]
39. Bharti, S.; Sharma, L.; Sahoo, B.K.; Malkar, P.; Srivastava, R. Application of relativistic coupled cluster theory to elastic scattering of electrons from confined Ca atoms. *J. Phys. B* **2019**, *52*, 185003. [CrossRef]
40. Gribakin, G.F.; Ludlow, J. Convergence of partial-wave expansions for energies, scattering amplitudes and positron annihilation rates. *J. Phys. B At. Mol. Opt. Phys.* **2002**, *35*, 339. [CrossRef]
41. Chakraborty, A.; Rithvik, S.K.; Sahoo, B.K. Relativistic normal coupled-cluster theory analysis of second- and third-order electric polarizabilities of Zn I. *Phys. Rev. A* **2022**, *105*, 062815. [CrossRef]
42. Newton, R.G. *Scattering Theory of Waves and Particles*; Springer: Berlin/Heidelberg, Germany, 1982.
43. Estevez, G.; Bhuiyan, L.B. Electrostatic potential due to a Fermi-type charge distribution. *Am. J. Phys.* **1985**, *53*, 450–453. [CrossRef]
44. Hara, S. The Scattering of Slow Electrons by Hydrogen Molecules. *J. Phys. Soc. Jpn.* **1967**, *22*, 710–718. [CrossRef]
45. Arretche, F.; Barp, M.V.; Tenfen, W.; Seidel, E.P. The Hidden Ramsauer-Townsend Effect in Positron Scattering by Rare Gas Atoms. *Braz. J. Phys.* **2020**, *50*, 844–856. [CrossRef]
46. Burrow, P.; Michejda, J.; Comer, J. Low-energy electron scattering from Mg, Zn, Cd and Hg: Shape resonances and electron affinities. *J. Phys. B At. Mol. Phys.* **1976**, *9*, 3225. [CrossRef]
47. Sahoo, B.K.; Das, B.P. Relativistic coupled-cluster studies of dipole polarizabilities in closed-shell atoms. *Phys. Rev. A* **2008**, *77*, 062516. [CrossRef]
48. Singh, Y.; Sahoo, B.K. Correlation trends in the polarizabilities of atoms and ions in the boron, carbon, and zinc homologous sequences of elements. *Phys. Rev. A* **2014**, *90*, 022511. [CrossRef]
49. Singh, Y.; Sahoo, B.K. Rigorous limits on the hadronic and semileptonic CP-violating coupling constants from the electric dipole moment of ^{199}Hg. *Phys. Rev. A* **2015**, *91*, 030501(R). [CrossRef]
50. Prasannaa, V.S.; Mitra, R.; Sahoo, B.K. Reappraisal of P, T-odd parameters from the improved calculation of electric dipole moment of ^{225}Ra atom. *J. Phys. B* **2020**, *53*, 195004. [CrossRef]
51. Sahoo, B.K.; Das, B.P. Relativistic Normal Coupled-Cluster Theory for Accurate Determination of Electric Dipole Moments of Atoms: First Application to the ^{199}Hg Atom. *Phys. Rev. Lett.* **2018**, *120*, 203001. [CrossRef]
52. Corzo, H.H.; Sehanobish, A.; Kara, O. Learning Full Configuration Interaction Electron Correlations with Deep Learning. *arXiv* **2021**, arXiv:2106.08138.
53. Zaklika, J.; Hładyszowski, J.; Ordon, P.; Komorowski, L. From the Electron Density Gradient to the Quantitative Reactivity Indicators: Local Softness and the Fukui Function. *ACS Omega* **2022**, *7*, 7745–7758. [CrossRef] [PubMed]
54. Diouf, Y.; Talla, K.; Diallo, S.; Gomis, L. Numerical Study of Density Functional Theory of Multi-electronic Atoms: Case of Carbon and Helium. *Am. J. Nanomaterials* **2021**, *9*, 12–22. [CrossRef]
55. Thakkar, A.J.; Lupinetti, C. Atomic Polarizabilities and Hyperpolarizabilities: A Critical Compilation. In *Computational, Numerical and Mathematical Methods in Sciences and Engineering*; Maroulis, G., Ed.; 2006; Volume 1, Chapter 4, pp. 505–529. Available online: https://www.worldscientific.com/doi/abs/10.1142/9781860948862_0014 (accessed on 24 July 2022).
56. Porsev, S.G.; Derevianko, A. High-accuracy calculations of dipole, quadrupole, and octupole electric dynamic polarizabilities and van der Waals coefficients C_6, C_8, and C_{10} for alkaline-earth dimers. *J. Expt. Theor. Phys.* **2006**, *102*, 195–205. [CrossRef]
57. Singh, Y.; Sahoo, B.K.; Das, B.P. Correlation trends in the ground-state static electric dipole polarizabilities of closed-shell atoms and ions. *Phys. Rev. A* **2013**, *88*, 062504. [CrossRef]
58. Schwerdtfeger, P.; Nagle, J.K. 2018 Table of static dipole polarizabilities of the neutral elements in the periodic table. *Mol. Phys.* **2019**, *117*, 1200–1225. [CrossRef]
59. Huot, J.; Bose, T.K. Experimental determination of the dielectric virial coefficients of atomic gases as a function of temperature. *J. Chem. Phys.* **1991**, *95*, 2683–2687. [CrossRef]
60. Taylor, P.R.; Lee, T.J.; Rice, J.E.; Almlöf, J. The polarizabilities of neon. *Chem. Phys. Lett.* **1989**, *163*, 359–365. [CrossRef]
61. Johnston, D.R.; Oudemans, G.J.; Cole, R.H. Dielectric Constants of Imperfect Gases. I. Helium, Argon, Nitrogen, and Methane. *J. Chem. Phys.* **1960**, *33*, 1310–1317. [CrossRef]
62. Hohm, U.; Kerl, K. Interferometric measurements of the dipole polarizability α of molecules between 300 K and 1100 K. *Mol. Phys.* **1990**, *69*, 803–817. [CrossRef]

63. Cernusak, I.; Diercksen, G.H.F.; Sadlej, A.J. Multipole polarizabilities of Ar. *Chem. Phys. Letts.* **1986**, *128*, 18–24. [CrossRef]
64. Maroulis, G.; Bishop, D.M. On the electric polarisabilities of argon. *J. Phys. B At. Mol. Phys.* **1985**, *18*, 4675. [CrossRef]